ISSN: 2643-6876

Current Trends in Civil & Structural Engineering

DOI: 10.33552/CTCSE.2026.12.000778

Iris Publishers

Review Article

Modeling the compressive behavior and cracking process of plain concrete (PC) and fiber reinforced concrete (FRC)

Pierre Rossi*

Civil Engineering Department, COPPE, Federal University of Rio de Janeiro, Brazil

***Corresponding author:** Pierre Rossi, Civil Engineering Department, COPPE, Federal University of Rio de Janeiro, Brazil

Received Date: December 05, 2025

Published Date: January 12, 2026

Abstract

This paper investigates the complex cracking process of PC and FRC under compression. It outlines a six-step mechanism describing crack evolution, highlighting the role of heterogeneity, Poisson's effect, and friction. The study also analyzes the impact of boundary conditions in standard tests and evaluates the bridging effect of fibers. Probabilistic Semi-Explicit Cracking models for PC (PSEC) and FRC (PSEC^f) are proposed to capture the distinct behaviors observed in compression and more especially the oblique cracks creation.

Keywords: Concrete, Fiber-Reinforced Concrete, Compression, Cracking Process, Boundary Conditions, Probabilistic Models, Finite Element Modeling

Introduction

The compressive behavior of concrete, along with its Young's modulus, is a fundamental mechanical property. Compressive strength has long been standardized and is widely used in both design codes and nonlinear finite element modeling. However, the cracking behavior of PC, and particularly FRC, is significantly more complex than typically assumed. This paper presents a detailed examination of this cracking process and introduces Probabilistic Semi- Explicit Cracking models for PC (PSEC) and FRC (PSEC^f). These models aim to analyze the propagation of macrocracks in structures subjected to predominantly compressive stresses.

PC cracking process under compression

The cracking process of PC and FRC under compression has been the subject of very detailed descriptions in the past [1,2]:

- **Step 1: Initiation and propagation of diffuse microcracking**

Tensile stresses, induced by Poisson's effect and the material's heterogeneity, lead to microcracks parallel to the loading direction. These small openings do not affect the specimen's elastic behavior.

- **Step 2: Formation of long vertical cracks**

Microcracks evolve into long vertical cracks, which segment the specimen into slender columns. Despite this segmentation, the material remains quasi-linear elastic due to the elastic behavior of these columns.

- **Step 3: Formation of oblique microcracks**

Irregular geometries and local bending within columns create oblique microcracks (due to local tensile stresses insides the col-

umns). These remain small and do not significantly alter global mechanical behavior.

- **Step 4: Onset of oblique mesocrack propagation**

Microcracks coalesce into oblique mesocracks (always due to local tensiles stresses). Tangential displacements and resulting friction introduce non-linear strain and energy dissipation.

- **Step 5: Localization of an inclined macrocrack**

One mesocrack dominates, forming an inclined macrocrack. This process consumes energy through friction and corresponds to the peak load of the compression test.

- **Step 6: Propagation of the inclined macrocrack**

Macrocrack propagation defines post-peak behavior. Friction during sliding leads to less brittle response compared to tension. Visible vertical crack openings result from tangential displacements. It is important to specify that the propagation of the inclined macrocrack is governed by local tensile stresses (mode I propagation), because, in concrete, cracks creation and propagation are always governed by local tensile stresses (due to the high material heterogeneity).

Influence of boundary conditions in standard compression tests

Frictional restraint at the specimen-press interface can distort stress fields and increase shear near the ends. This leads to excessive mesocrack formation, increased confinement, and artificially elevated compressive strength and ductility. This point was experimentally studied and demonstrated in the past [3,4].

Such artifacts must be carefully considered to avoid overestimating concrete performance. Fibers act by bridging active cracks with mode I or II displacements. Their effectiveness begins at Step 5 of the cracking process and is most pronounced during Step 6 [2]. Under ideal conditions, fibers enhance post-peak behavior but do not significantly raise compressive strength. However, in the presence of boundary condition artifacts, the apparent contribution of fibers is exaggerated due to increased crack formation near platens.

Modeling the compressive behavior: existing approaches

If the cracking process of concrete under compression is considered (as discussed in Chapters II, III and IV), several important observations emerge:

- The post-peak behavior is not an intrinsic material property, but rather a structural one.
- The boundary conditions imposed by experimental setups related to standard compression test tend to overestimate both the compressive strength and the ductility of concrete.
- Only the quasi-linear elastic portion of the experimental stress-strain curve, obtained from a compression test influenced by boundary effects, can be reliably considered as an intrinsic material property.

The issue lies in the fact that most compression tests used to characterize the compressive behavior of concrete, particularly standard test, are affected by these boundary conditions. As a result, the current methods for modeling compressive behavior are highly questionable.

Two main modeling approaches are commonly found in the literature:

- Analytical formulations in design codes (e.g., Eurocode 2)
- Finite element models

The first approach is based on the well-established concept of cracked section equilibrium. In this case, a simplified model curve is arbitrarily derived from the experimental curve,

incorporating safety factors that significantly under estimate the compressive response observed in tests. Consequently, up to the peak load, this standard approach can generally be considered conservative.

The second category includes smeared cracking models and damage models [5–13], which are more widely used in numerical simulations. These models typically rely on stress–strain laws calibrated directly from experimental data, including the post-peak portion of the curve. However, if the findings from previous chapters are considered, this method of fitting model parameters is fundamentally flawed, as it misrepresents the material's true behavior.

PSEC and PSEC^f models

PSEC model

In this proposed model, macrocrack propagation is governed by two key criteria:

- Macrocrack initiation is associated with the uniaxial tensile strength f_t,
- Macrocrack propagation is governed by the mode I critical fracture energy G_{IC}, as defined in the well-known Linear Elastic Fracture Mechanics (LEFM) framework.

A macrocrack propagates when the entire G_{IC} is dissipated, and the crack is numerically represented as a sequence of fully damaged finite elements. The novelty of this approach lies in its use of volume elements, rather than singular elements typically employed in conventional LEFM-based numerical models. Therefore, the proposed model does not fall under the category of classical damage or smeared crack models.

In classical damage models, damaged zones are treated as physically real, and crack openings are derived from these zones. In contrast, the proposed model does not consider physically existing damaged zones. Instead, a damage parameter is introduced arbitrarily as a mechanism to dissipate GIC, without representing a physically observable phenomenon.

The mechanical properties f_c and G_{IC} are treated as random variables that depend on the size of the mesh elements. Previous experimental and numerical studies [14,15] have established and

validated their probabilistic behavior. These properties are linked to the element heterogeneity ratio, re r_e>1, defined by:

$$r_e = V_e / V_a \quad (1)$$

Where, V_a is the volume of the greatest aggregate size of concrete and V_e is the volume of the mesh element.

The probabilistic properties of f_t and G_{IC}, it means the mean value, μ, and σ, the standard deviation, are given by the following relations:

$$\mu\left(f_t\left(r_e\right)\right) = a\left(r_e\right)^{-y} \quad (2)$$

In Equation (2), a = 6.5 MPa and y is given by Equation (3), were f_c represents the concrete compressive strength in MPa and α = 1 MPa. The compressive strength is determined by performing a standard test on 160 x 320 mm cylinder specimen.

$$y = 0.25 - 3.6\times10^{-3} f_c/\alpha + 1.3\times10^{-5}\left(f_c/\alpha\right)^2 \quad (3)$$

$$\sigma/\mu\left(f_t\left(r_e\right)\right) = c\left(r_e\right)^{-d} \quad (4)$$

In Equation (4), c = 0.35 and d is given by Equation (5), as follows:

$$d = 4.5\times10^{-2} + 4.5\times10^{-3} f_c/\alpha - 1.8\times10^{-5}\left(f_c/\alpha\right)^2 \quad (5)$$

A schematic overview of the model is provided in Figure 1.

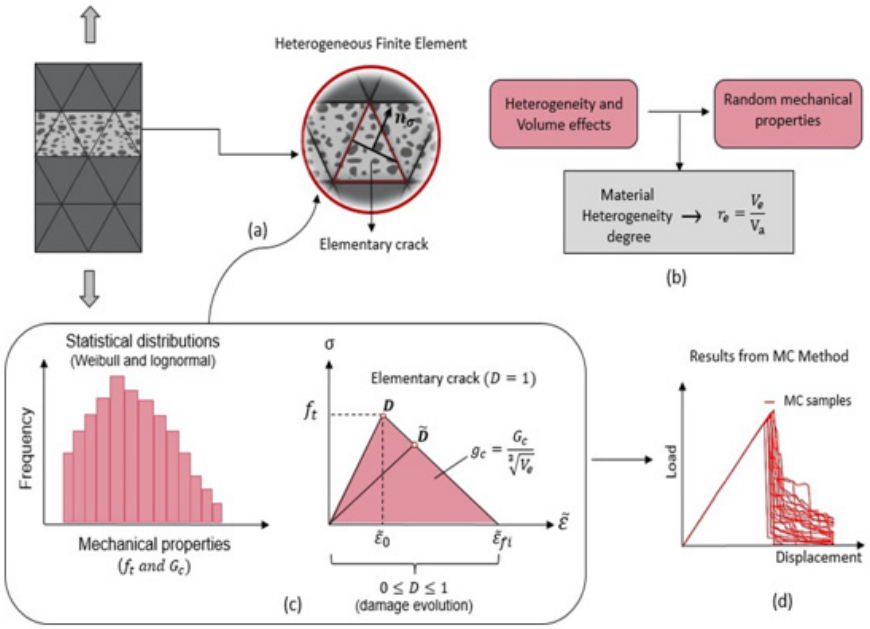

Figure 1: General aspects of the 3D probabilistic semi-explicit cracking model of concrete [15].

As shown in Figure 1, the introduction of a damage parameter in the theoretical approach is arbitrary and serves solely as a method to dissipate G_{IC}. It means that, in the proposed model, there is no relation between the non-linear strain (softening branch of the stress-strain curve in tension) and a real crack propagation.

Finally, it is important to point out that it has been demonstrated that the 3D probabilistic semi-explicit cracking model is mesh independent in static if r_e>1 [15].

PSEC^f model

The basis of the PSEC^f model was initially introduced for the simulation of large-scale FRC structures under static loading conditions [16]. This model is specifically developed to simulate the propagation of macrocracks and is grounded in the uniaxial tensile behavior of FRCs. It applies only to FRCs that exhibit softening behavior in post-cracking uniaxial tension.

The primary aim of the PSEC^f model is to overcome a significant limitation of conventional distributed cracking models [17–23], namely their tendency to generate overly dispersed crack patterns. This dispersion often leads to a substantial underestimation of dominant crack openings [16]. The PSEC^f model addresses this issue by simulating macrocrack initiation and propagation through linear volumetric finite elements. A crack is assumed to form when the tensile stress at an element's integration point (there is only one

point of integration in the finite tetrahedron element used, located at the centroid of the element) exceeds the matrix tensile strength (i.e., the tensile strength of the unreinforced concrete), under the assumption of a perfectly brittle matrix.

The matrix tensile strength is treated as a random variable that follows a Weibull distribution (as for the PSEC model), with its statistical properties depending on the volume of the finite element. As the element volume increases, both the mean and standard deviation of the tensile strength decrease, reflecting the size effect observed in quasi-brittle materials.

Experimental results reported in [24] indicate that the average post-cracking energy associated with fiber bridging is independent of the tested material volume, although its standard deviation decreases with increasing volume. To reflect this behavior and simplify implementation, the PSEC^f model treats the fiber bridging energy, denoted G_{wf}, as a deterministic parameter, assumed to be independent of the finite element volume.

The model distinguishes two key mechanical stages:

- Macrocrack initiation, governed by the tensile strength of the matrix.
- The fiber bridging effect, which controls the post-crack energy dissipation.

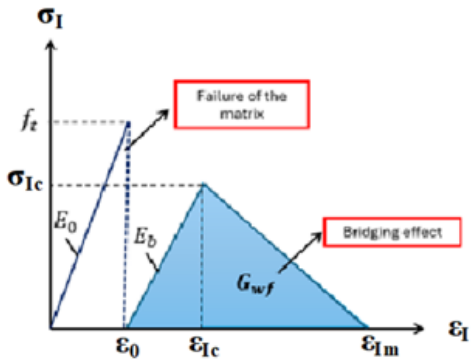

Figure 2: Aspects of the PSEC^f model for fiber-reinforced concrete – Mechanical behavior in uniaxial tension.

Crack initiation in the PSEC^f model occurs when the maximum principal tensile stress σ_I in a finite element reaches (at the center of gravity of the element) its randomly assigned tensile strength f_t. At this point, the element's stiffness undergoes a sharp reduction, indicating the onset of cracking. During the fiber bridging phase, as the maximum principal strain ε_I increases, the bridging mechanism becomes active. This results in an increase in effective stiffness Eb, though it remains below the original undamaged stiffness E_0. As crack opening continues and ε_I reaches a critical strain ε_{Ic}, the stress σ_I begins to decrease linearly with further strain, representing the fiber pullout process. When the strain reaches a maximum value ε_{Im}, the bridging effect of the fibers is considered negligible, and the element stiffness is reduced to zero.

This softening behavior is modeled through a simplified damage-based approach, wherein only the entries of the stiffness matrix associated with the direction of σ_I (i.e., the maximum principal stress-strain relation) are modified. All other matrix components remain unchanged. As a result, the fiber bridging effect is treated as anisotropic, reflecting the directional nature of crack propagation.

A key advantage of this approach is the improved localization of cracks. Since the concrete matrix is assumed to behave as perfectly brittle, and its tensile strength is treated as a random variable, the model is able to represent crack initiation and propagation more realistically than smeared (diffuse) cracking models, which tend to artificially spread damage over large areas. It is important to note that the PSEC^f model is not applicable to FRCs that exhibit hardening behavior in uniaxial tension.

In this model, the fiber bridging effect is only activated when the matrix is fully cracked. While this simplification may seem restrictive in light of the macroscopic response observed in direct tensile tests on notched specimens, it is deliberately chosen for physical consistency. In such tests, a softening response is observed, attributed to the propagation of a macrocrack and the gradual engagement of fibers across the cracked section. However, this macrocrack propagation phase does not reflect an intrinsic material property, but rather a structural effect, which depends on specimen geometry, particularly the cross-sectional area at the crack location [1].

Therefore, the PSEC^f model isolates and represents only the two intrinsic material stages in the tensile behavior of FRC:

- The pre-cracking response, up to the peak load, representing the behavior of uncracked FRC, and
- The post-cracking fiber bridging response, which governs the load transfer after the entire cross-section, is fully cracked.

Importantly, it has been experimentally demonstrated [24] that the mean post-cracking behavior due to fiber bridging is independent of specimen size, though its scatter decreases with increasing specimen dimensions. Hence, an appropriate number of specimens must be tested to obtain a reliable estimate of the average bridging behavior [24].

Parameters determination of the PSEC^f

The mean tensile strength of the matrix ft and its standard deviation (which depends on the finite element volume) are computed from previously validated formulas (chapter 5.1). These properties are randomly distributed across the mesh following a Weibull distribution.

The fiber bond energy G_{wf} is derived from uniaxial tensile test on notched specimens [25]. Since this uniaxial tensile test measure crack opening, a conversion to strain is necessary for modeling and numerical simulations. This conversion involves dividing the crack opening by a characteristic length of the finite elements, $l_e = V_e^{(1/3)}$, where Ve represents the volume of the finite element.

An example of test set-up related to the direct tensile test on notched specimen is presented in following. This test set-up has long been validated [1,26].

A very good technical solution is to use, as connection between the specimen and the testing machine, aluminum cylinders having the same diameter than the specimen tested. Aluminum having a young modulus/Poisson ratio close to that of concrete, stress concentration in the glue (which serves to connect the specimen to the aluminum bar) and in the specimen near the connection is very low. These aluminum cylinders are directly screwed on the testing machine.

A schematic draw of this test set-up is presented in Figure 3.

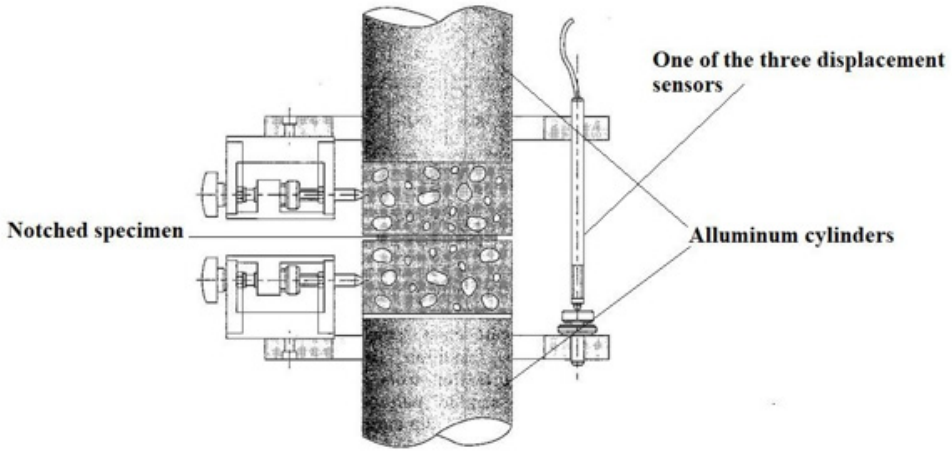

Figure 3: Schematic draw of the bond between the notched specimen and the aluminum cylinders – vertical cut (from [1]).

To minimize this stress concentration, the length of the aluminum cylinders is chosen in relation with the length of the dimensions of the specimen. This length optimization of the aluminum cylinders is made by performing linear finite element analysis (considering both the specimen and the aluminum cylinders).

Determination of the tensile stress-crack opening curve useful to calculate G_{wf}

As précised before, when a notched specimen is concerned, the beginning of the test is related to a macrocrack propagation along the specimen section (at the level of the notch).

This propagation coincides with a local bending inside the cracked section. This bending can occur until the complete macrocrack creation. Therefore, the part of the tensile stress-crack opening curve related to this step of crack propagation has not to be considered.

The crack is considered completely open along the section of the specimen when all displacement sensors indicate an opening displacement, w^0, equal to 10^{-4}. L_s. L_s is the basis length of measurement of the sensors and 10^{-4} corresponds to a conventional value of cracking strain of concrete.

After the step of crack propagation, the local bending is less if the test is well performed, whether with the gripping or the bonding connection.

Only when w_0 is reached for all displacement sensors, an average crack opening can be considered. The smaller average crack opening is called w_i.

Figure 4 illustrates how w_0 and w_i are determined (case of bounding connection).

Consequently, G_{wf} is calculated considering the experimental

stress-crack opening curve from the crack opening w_i. It means that for crack openings inferior to w_i the fibers bridging effect is not considered. This approximation leads to a conservative numerical simulation with respect to the actual behavior of the structure under consideration.

In practice, a number of uniaxial tests need to be conducted to determine the average value of G_{wf} to be used in the numerical simulations.

Determination of ε_{1c}, σ_{1c} and ε_{1m}

σ_{1c} is determined directly from the experimental average tensile stress-crack opening curve. It is the maximal average value of the post-cracking tensile strength. Concerning ε_{1c}, it is more complicated. The fiber bridging effect being only considered from an experimental crack opening equal to w_i, while, in the numerical model, this bridging effect begins at zero crack opening, it is clear that the value of w_{1c} (and so of ε_{1c}) considered in the numerical model (w_{Icn}) has to be lower than that observed in the experiment (w_{Ice}).

This value of w_{Icn} can be calculated considering this point: the experimental bridging effect attributable to a material behavior starts when the volume of the macrocracks is equal to ($w_i \cdot S_p$), where S_p is the cracked section of the specimen, while the numerical bridging effect starts when the volume element is fully cracked (its rigidity matrix is equal to 0). To get an equivalent bridging effect between the numerical model and the experiment, the following relation as to be considered (as approximation):

$$W_{Icn} = W_{Ice}\left(\left(w_i \cdot S_p / V_e\right)\right) \tag{6}$$

ε_{1m} is calculated as following:

$$\varepsilon_{1m} = 2\,G_{wf} / \sigma_{Ic} + \varepsilon_0 \tag{7}$$

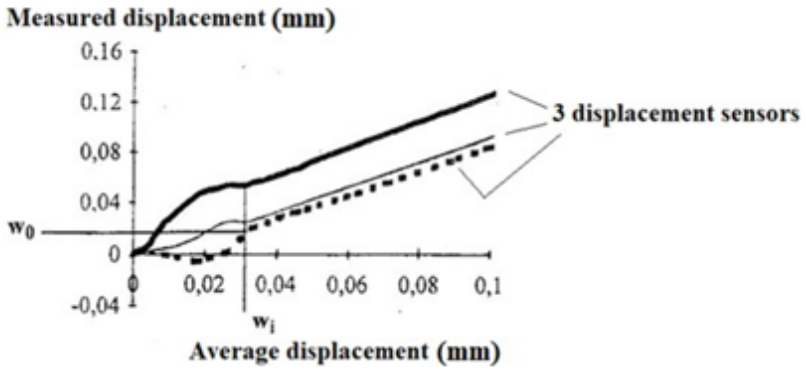

Figure 4: Example of determination of and (from [1]).

It is important to emphasize that, due to the probabilistic nature of both the PSEC and PSEC^f models, a Monte Carlo simulation procedure is essential to generate results that accurately capture the inherent variability in both model parameters and material properties. For a given structural configuration, the resulting ensemble of simulations enables statistically robust analyses, supporting reliability-based or safety-oriented assessments of structural performance.

One must finally point out that the PSEC model has been the subject of a numerical implementation validated by experimental results, whereas the PSEC^f model remains a proposed approach, for which numerical implementation and validation are yet to be carried out.

However, in their current formulations, the PSEC and PSEC^f models are limited to simulating crack propagation under predominantly tensile stress states. They do not account for cracking driven by compressive stresses, which is the primary focus of the present work. This limitation necessitates further model development, which is addressed in the following chapter.

PSEC and PSEC^f models for macrocracks propagation under predominant compressive stress

It is clear that the PSEC and PSEC^f models, which are macroscopic in nature, are neither intended nor capable of representing all the stages of the cracking process in concrete and fiber reinforced concrete described in Chapters II, III, and IV. However, it is important that they are able to account for the onset of the inclined macrocrack that leads to the ultimate compressive strength of concrete.

Although the initiation of this inclined macrocrack results from the presence of local tensile stresses at various scales within the compressive cracking process, it is essential that both models incorporate the initiation of this inclined macrocrack.

At the macroscopic scale of a finite element volume, this inclined crack can be interpreted as a shear crack. Therefore, introducing a shear-based criterion to initiate this inclined crack in concrete is a relevant and justified approach.

Referring to the Mohr-Coulomb failure criterion, it appears evident that the shear strength should be equal to $f_t/2$. This shear strength is thus treated as a deterministic parameter, in contrast to the tensile strength, which is considered a random variable dependent on the finite element volume. This choice of using a deterministic parameter is consistent with the cracking process of concrete under compression described in Chapter II. Unlike the tensile cracking process, the compressive cracking process is not governed by the presence of the weakest element, as suggested by Weibull's weakest link theory [27,28].

Consequently, both models incorporate two criteria for macrocrack initiation: a tensile criterion, and a shear criterion.

For the shear criterion, as with the tensile one, the model considers the maximum principal shear stress τ_I (always at the centroid of the element). The two initiation criteria are therefore expressed as:

$$\begin{cases} \sigma_I - f_t \geq 0 \text{macrocrack initiation in Tension} \\ \tau_I - \dfrac{f_c}{2} \geq 0 \text{macrocrack initiation in Shear} \end{cases} \quad (8)$$

Of course, it is possible for both criteria to be satisfied simultaneously within the same element. However, only one macrocrack should be initiated per element. Therefore, a selection rule must be applied to determine which criterion governs the crack initiation.

One way to make this decision is to consider the dominant criterion, defined as follows:

$$\begin{cases} \left[(\sigma_I - f_t)/f_t\right] - \left[(\tau_I - 0.5f_c/0.5f_c)\right] \geq 0, \text{tension is dominate} \\ \left[(\sigma_I - f_t)/f_t\right] - \left[\dfrac{\tau_I - 0.5f_c}{0.5} f_c\right] \leq 0, \text{shear is dominate} \end{cases} \quad (9)$$

In the unlikely case where:

$$\left[(\sigma_I - f_t)/f_t\right] - \left[\frac{\tau_I - 0.5f_c}{0.5} f_c\right] = 0, \text{the tensile criterion is selected} \quad (10)$$

If the macrocrack is initiated in shear, the angle of this crack within a finite element is determined based on the direction of the maximum principal shear stress. The orientation of the macrocrack serves as essential initial information for modeling its post-localization behavior within both probabilistic models.

In the case of the PSEC model, the propagation of the inclined crack occurs in Mode I, i.e., it is governed by local tensile stresses, as previously described.

In the case of the PSEC^f model, the propagation phase of the macrocrack is not considered, as the matrix is assumed to be elastic perfectly brittle. Only the bridging effect of the fibers is considered. Given that the tensile stiffness of the fibers is significantly higher than their shear stiffness, only the bridging effect in tension is modeled.

Consequently, in both probabilistic models, only the tensile behavior in the direction perpendicular to the inclined crack is considered.

From a numerical computation perspective, this is implemented within a finite element as follows:

1. The inclination angle of the initiated macrocrack is stored.
2. The tensile stress perpendicular to the direction of the inclined macrocrack is computed.
3. The evolution of this tensile stress as a function of the corresponding strain follows the constitutive law shown in Figure 1 for the PSEC model and the law shown in Figure 2 for the PSEC^f model.

It is important to emphasize that, for both the PSEC and PSEC^f models, the maximum principal shear stress can, theoretically (mechanically), have two orthogonal directions. Therefore, it is necessary to define a criterion to choose between these two directions. The method for making an objective choice remains to be proposed (and presented in a future paper).

The numerical implementations of both probabilistic models, as well as their experimental validation, remain to be carried out concerning the cracking behavior of PCs and FRCs.

It is nevertheless important to note that the use of a dual cracking criterion (in tension and in shear) has already been considered in the past in the development of probabilistic explicit cracking models (PEC models). These models account for cracking through the use of interface finite elements, as opposed to volume elements employed in the present work. These numerical models address both PCs (PEC model) and FRCs (PEC^f model), and have been experimentally validated [29, 30]. These prior works lend credibility to the numerical developments proposed in this article.

Conclusions

This work focuses on the modeling of macrocrack propagation in Plain Concrete (PC) and Fiber Reinforced Concrete (FRC) structures when this propagation is governed by predominantly compressive stresses. The modeling is based on two probabilistic models: the PSEC model (for PC structures), which has already been numerically implemented and experimentally validated, and the PSEC^f model (for FRC structures), which is currently under numerical implementation and validation. In their current state, both probabilistic models only account for macrocrack propagation governed by predominantly tensile stresses. This paper presents, in detail, their planned extension to compressive stress-driven cracking. These extensions are grounded in a precise and comprehensive analysis of the compression-induced cracking process in PC and FRC. The physical foundations of these two probabilistic models constitute their originality and relevance,

making them valuable tools for both the scientific community and engineering applications.

References

1. Rossi P (1988) Les bétons de fibres, Les presses de l'Ecole Nationale des Ponts et Chaussées.
2. Rossi P (2023) True Compression Behavior of Concretes and Fiber Reinforced Concretes. Cur Trends Civil & Struct Eng 10(2).
3. Torrenti JM, Desrues J, Benaija EH, Boulay C (1991) Stereophotogrammetry and localization in concrete under compression. J Eng Mech 117(7): 1455-1465.
4. Torrenti JM, Benaija EH, Boulay C (1993) Influence of boundary conditions on strain softening in concrete compression test. J Eng Mech 119(12): 2369-2384.
5. Bazant ZP, Oh BH (1983) Crack band theory for fracture of concrete. Matériaux Constr 16: 155–177.
6. Mazars J (1984) Application de la mécanique de l'endommagement au comportement non- linéaire et la rupture du béton de structure. Ph.D. thesis, L.M.T.
7. Rots J, Nauta P, Kuster G, Blaauwendraad J (1985) Smeared crack approach and fracture localization in concrete, HERON 30(1).
8. Pijaudier Cabot G, Bazant ZP (1987) Nonlocal damage theory. J Eng Mech ASCE 113: 1512–1533.
9. Jirasek M, Zimmermann T (1998) Rotating crack model with transition to scalar damage. Journal of engineering mecchanics 124(3): 277–284.
10. Bazant Z, Jirasek M (2002) Nonlocal integral formulations of plasticity and damage: survey of progress. J Eng Mech 128: 1119-1149.
11. Oliver J, Huespe AE, Samaniego E, Chaves E (2004) Continuum approach to the numerical simulation of material failure in concrete. International journal for numerical and analytical methods in geomechanics 28 (7-8): 609–632.
12. Oliver J, Huespe AE (2004) Continuum approach to material failure in strong discontinuity settings. Computer methods in applied mechanics and engineering 193 (30-32): 3195-3220.
13. Jirasek M (2011) Damage and smeared crack models. G Hofstetter, G Meschke (Eds.), Numerical modeling of concrete cracking, Springer, p. 1–49.
14. P Rossi, X Wu, F Le Maou, A Belloc (1994) Scale effect on concrete in tension. Mater Struct 27: 437–444.
15. MR Rita, P Rossi, Ed MR Fairbairn, FLB Ribeiro (2024) Determination of the Probabilistic Properties of the Critical Fracture Energy of Concrete Integrating ScaleEffect Aspects. Appl Sci 14: 462.
16. Rossi P (2023) Basis of Probabilistic Semi-Explicit Cracking Model for Fiber Reinforced Concretes. Cur Trends Civil & Struct Eng 10(1).
17. Fanella D, Krajcinovic D (1985) Continuum damage mechanics of fiber reinforced concrete. J Eng Mech 111(8): 995-1009.
18. Li F, Li Z (2000) Continuum damage mechanics-based modeling of fiber reinforced concrete in tension. Int J Solids Struct 38: 777-793.
19. Peng X, Meyer C (2000) A continuum damage mechanics model for concrete reinforced with randomly distributed short fibers. Comput Struct 78: 505-515.
20. Barros J, Figueiras JA (2001) Model for the analysis of steel fiber reinforced concrete slabs on grade. Computers & Structures 79(1): 97-106.
21. Cunha V, Barros J, Sena Cruz J (2012) A finite element model with discrete embedded elements for fiber reinforced composites. Computers & Structures 94-95: 22-33.
22. De Montaignac R, Massicotte B, Charron JP (2013) Finite-element modelling of SFRC members in bending. Magazine of Concrete Research 65(19): 1133-1146.
23. Lagier F, Massicotte B, Charron JP (2016) 3D Nonlinear Finite-Element Modeling of Lap Splices in UHPFRC. Journal of Structural Engineering 142(11).
24. Rossi P (2012) Experimental Study of Scaling Effect Related to Post-Cracking Behaviors of Metal Fibers Reinforced (MFRC). European Journal of Environmental and Civil Engineering 16(10): 1261-1268.
25. (2001) RILEM TC 162. Test and design methods for steel fibre reinforced concrete: Uniaxial tension test for steel fibre reinforced concrete. Mater Struct 34(235): 3–6.
26. Casanova P, Rossi P (1997) Analysis and design of steel fiber reinforced concrete beams. ACI Structural Journal 94(5): 595-602.
27. Weibull W (1939) A Statistical Theory of the Strength of Materials, Royal Swedish Institute for Engineering Research: Stockholm, Sweden.
28. Weibull W (1951) A statistical distribution function of wide applicability. J Appl Mech 18: 293–297.
29. Phan TS, Tailhan JL, Rossi P (2013) 3D numerical modelling of concrete structural element reinforced with flat steel rebars. Structural Concrete 14(4): 378-388.
30. Rossi P, Tailhan JL, Daviau Desnoyer D (2016) Numerical models for designing steel fiber reinforced concrete structures: why and which ones? ACI Special Publication, FIB Bulletin 79 - ACI SP-310, pp.289-300.